Table IV. Atomic Valency Values Obtained with the Present Method for Different States of HCN[a]

molecule	state	V_C	V_N	V_H
HCN	$^1A'$	(3.98)	(3.01)	(0.99)
HCN	$^3A''$	3.04	2.12	0.96
HCN^-	$^2A''$	3.28	2.37	0.90
		(3.23)	(2.33)	(0.96)

[a] Values in parentheses are the actual atomic valencies obtained with the STO-3G wave function.

atomic valency values for HCN^- calculated by the present procedure (using the wave function for HCN) and that obtained from the SCF wave function for HCN^- are in good agreement (see Table IV). Hence one may use the present simple procedure to obtain atomic valencies in various electronic states.

The effect of electronic excitation on atomic valencies may be illustrated by considering HCN. According to the valency prediction, $1a'' \rightarrow 7a'$ excitation (i.e., $^1A'$ state to $^3A''$ state) leads to a significant bending of the molecule (see Table III). There is considerable reduction in the valencies of C and N (Table IV) and consequent weakening of the C–N bond. In HCN^-, with a bond angle of 145°, valencies of C and N are again reduced, though not to the same extent as in the $^3A''$ state of HCN. It would be interesting to apply the present method to study the changes in atomic and interatomic valency on molecular excitation and ionization and correlate them with reactivity, strain, and the radical nature of excited species.

VI. Conclusions

The general criteria for a molecular orbital quantity to serve as a successful Walsh ordinate in the sense of giving correct qualitative predictions of molecular shape are formulated as follows. The sign and relative magnitude of the slopes of a given MO should remain the same for different molecules of a particular symmetry species and the core and lone pair orbitals should not be affected by bond angle variation. We have studied how well the two ordinates, the recently proposed MO valency and the commonly used MO eigenvalue, satisfy these criteria. It is found that both of these ordinates are suitable for the generation of universal correlation diagrams, which are in reasonable agreement with the original Walsh diagrams. It is, however, noted that core and lone pair orbital eigenvalues vary considerably with bond angle, in contrast to the original Walsh diagrams and the present valency correlation diagrams.

The fact that MO valency and MO eigenvalue correlation diagrams are similar does not imply that both would lead to the same quantitative bond angle predictions. It is the actual magnitudes of the slopes that are important for predicting the correct bond angle. The sum of eigenvalues often leads to serious errors in bond angle predictions, its plot as a function of bond angle exhibiting no minimum in several cases. In contrast, molecular valency, defined as the sum of molecular orbital valencies, predicts the ground-state bond angles to a fair degree of accuracy.

This finding is relevant when applied to the prediction of bond angles of excited states of molecules, which are not easily calculated otherwise. In this paper, we have proposed a simple valency method to determine equilibrium bond angles of any electronically excited, ionized, or reduced state of a molecule purely from its ground-state wave function. It is seen that this method gives results that are in good agreement with values obtained from CI calculations. Further, valencies of atoms in excited states of molecules can also be determined with this method. These atomic valencies might be of use in predicting the reactivity, strain, and radical nature of molecules in the excited states.

Band Electronic Structure Study of the Semimetallic Properties and the Anisotropic Resistivity Hump in $ZrTe_3$

Enric Canadell,*[1a] Yves Mathey,[1b] and Myung-Hwan Whangbo*[1c]

Contribution from the Laboratoire de Chimie Théorique and Laboratoire de Spectrochimie des Elements de Transition, Université de Paris-Sud, 91405 Orsay, France, and the Department of Chemistry, North Carolina State University, Raleigh, North Carolina 27695-8204.
Received June 1, 1987

Abstract: Tight-binding band calculations were carried out on $ZrTe_3$ to examine its semimetallic properties and anisotropic resistivity hump at ~63 K. Our calculations show that adoption of the type B structure is crucial for the semimetallic nature of $ZrTe_3$. The overlapping of the Te 5p-block bands with the Zr 4d-block bands gives rise to a pair of nested electron pockets and a pair of nested hole pockets, all of which have the shape of a flat cylinder whose axis is perpendicular to the chain direction. Thus, a charge density wave formation associated with the Fermi surface nesting does not affect the electrical conductivity of $ZrTe_3$ along the chain direction, so that the resistivity hump is observed only along the directions perpendicular to the chain axis.

Transition-metal trichalcogenides MX_3 (M = Ti, Zr, Hf; X = S, Se, Te)[2] consist of layers of composition MX_3. Each MX_3 layer is made up of trigonal-prismatic MX_3 chains, in which each X_3 triangle has a shape with one side much shorter than the other two. This leads to the oxidation formalism $(X^{2-})(X_2^{2-})$ for X_3[3] so that the formal oxidation state of the metal is M^{4+} (d^0), and thus the metal d-block bands of MX_3 are expected to be empty. In agreement with this prediction, all MX_3 compounds except for $ZrTe_3$ are found to be semiconductors with band gaps ranging from ~1 to ≳2 eV.[2b,4] If the electronic structure of $ZrTe_3$ is

(1) (a) Laboratoire de Chimie Théorique, Université de Paris-Sud. (b) Laboratoire de Spectrochimie des Elements de Transition, Université de Paris-Sud. Present address: Département de Physique, Faculté de Sciences de Luminy, 13288 Marseille. (c) Department of Chemistry, North Carolina State University.

(2) (a) Meerschaut, A.; Rouxel, J. *Crystal Structures and Properties of Materials with Quasi-One-Dimensional Structures*; Rouxel, J., Ed.; Reidel: Dordrecht, The Netherlands, 1986; p 222. (b) Bullett, D. W. *Theoretical Aspects of Band Structures and Electronic Properties of Pseudo-One-Dimensional Solids*; Kamimura, H., Ed.; Reidel: Dordrecht, The Netherlands, 1985, p 163. (c) Hulliger, F. *Structural Chemistry of Layer-Type Phases*; Lévy, F., Ed.; Reidel: Dordrecht, The Netherlands, 1976; p 247.

(3) Whangbo, M.-H. *Crystal Structures and Properties of Materials with Quasi-One-Dimensional Structures*; Rouxel, J. Ed.; Reidel: Dordrecht, The Netherlands, 1986; p 27.

(4) (a) Brattas, L.; Kjekshus, A. *Acta Chem. Scand.* **1972**, *26*, 3441. (b) Kurita, S.; Straehli, J. L.; Guzzi, M.; Lévy, F. *Physica* **1981**, *105B*, 169. (c) Herr, S. L.; Brill, J. W. *Synth. Metals* **1986**, *16*, 283. (d) Khumalo, F. S.; Olson, C. G.; Lynch, D. W. *Physica* **1981**, *105B*, 163. (e) Grimmeiss, H. G.; Rabenau, A.; Hahn, H.; Neiss, P. *Z. Elektrochem.* **1961**, *65*, 776. (f) Schairer, W.; Shafer, M. W. *Phys. Status Solidi.* **1973**, *A17*, 181. (g) Khumalo, F. S.; Hughes, H. P. *Phys. Rev.* **1980**, *B4*, 2078. (h) Perluzzo, G.; Jandl, S.; Girard, P. E. *Can. J. Phys.* **1980**, *58*, 143. (i) Nee, S. F.; Nee, T. W.; Fan, S. F.; Lynch, D. W. *Phys. Status Solidi.* **1982**, *B113*, K5.

0002-7863/88/1510-0104$01.50/0

similar to that of any other semiconducting MX_3, the metallic properties[5] of $ZrTe_3$ may be considered to originate from the presence of Te vacancies.[6] However, reflectance spectra of $ZrTe_3$ show that it is a semimetal[4c,7] thereby implying that the d-block bands of Zr overlap with the p-block bands of Te.

The electrical conductivities of $ZrTe_3$ are pseudo-two-dimensional (2D),[8] i.e., they are nearly isotropic in the plane of the $ZrTe_3$ layers such that $\sigma_b \cong \sigma_a > \sigma_{c^*}$. Here the *b*, *a*, and *c** axes are parallel to the chain, interchain, and interlayer directions, respectively. The resistivity versus temperature plot for $ZrTe_3$ exhibits a hump at ~63 K[8] so that a charge density wave (CDW) appears to be present in $ZrTe_3$. Interestingly, however, this resistivity hump is not observed along the chain direction but along the directions perpendicular to the chain.[8] In addition, $ZrTe_3$ is found to become a superconductor at 2 K.[9] In order to understand why $ZrTe_3$ is so different from other MX_3 chalcogenides in physical properties, we examine the electronic structure of $ZrTe_3$ by carrying out tight-binding band calculations[10] based upon the extended Hückel method.[11] In analyzing the band electronic structure of $ZrTe_3$, it is essential to recognize certain structural characteristics of $ZrTe_3$. Thus in the following we first describe the crystal structure of $ZrTe_3$ and then examine its band electronic structure. The atomic parameters employed in the present study are summarized in Table I.

Crystal Structure

Structures of layered transition-metal trichalcogenides MX_3 belong to type A (e.g., ZrS_3, $ZrSe_3$, HfS_3, $HfSe_3$) and/or to type B (e.g., TiS_3, ZrS_3, $ZrTe_3$, $HfSe_3$).[4a,12] So far, ZrS_3 and $HfSe_3$ are the only known compounds that exist in both type A and type B structures.[12a,b] Regardless of the MX_3 compounds chosen for comparison, it is observed to a very good approximation that the positional parameters, (x_A, y_A, z_A), of a type A structure are related to those, (x_B, y_B, z_B), of a type B structure as follows: $x_A = 1 - x_B$, $y_A = y_B$, and $z_A = z_B$.[12a] $ZrTe_3$ has a type B structure,[12a] as depicted in **1a** and **1b**. The hypothetical type A structure for

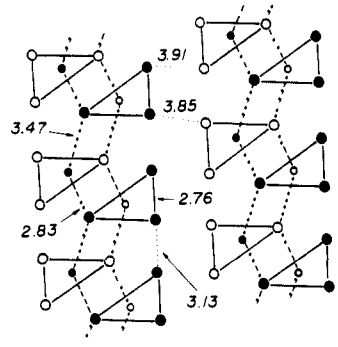

1a

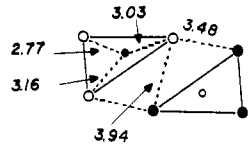

1b

Table I. Exponents and Parameters Used in the Calculations[a]

atom	orbital	H_{ii} (eV)	ζ_1	ζ_2	c_1[b]	c_2[b]
Zr	5s	−8.00	1.817			
	5p	−5.40	1.776			
	4d	−10.20	3.835	1.505	0.6210	0.5796
Te	5s	−20.78	2.510			
	5p	−13.20	2.160			

[a] A modified Wolfsberg–Helmholz formula[14] was used to calculate the off-diagonal H_{ij} values. [b] Contraction coefficients used in the double-ζ expansion.

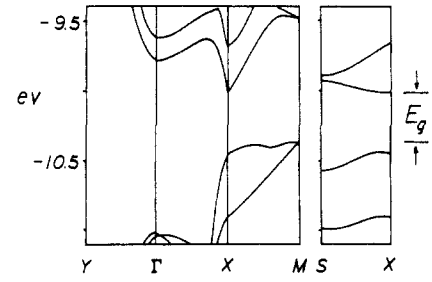

Figure 1. Dispersion relations of some bands in the vicinity of the band gap calculated for the type A structure of $ZrTe_3$. The valence and the conduction bands are largely composed of the Te 5p and the Zr 4d orbitals, respectively.

$ZrTe_3$, as obtained by the relationships $x_A = 1 - x_B$, $y_A = y_B$, and $z_A = z_B$, is illustrated in **2a** and **2b**. Comparison of the type A and type B structures shows that the following structural features are characteristic of the type B structure: (a) each triangular Te_3 unit of the trigonal prismatic chains is strongly distorted from an isosceles triangle; (b) between adjacent $ZrTe_3$ chains in each layer, there exist short Te···Te contacts (i.e., 3.48 Å in **1b**); (c) in each $ZrTe_3$ layer, long and short interchain Zr···Te distances (i.e., 3.47 and 2.83 Å) alternate between the chains; (d) short Te···Te contacts (i.e., 3.85 and 3.91 Å) are present between adjacent $ZrTe_3$ layers.

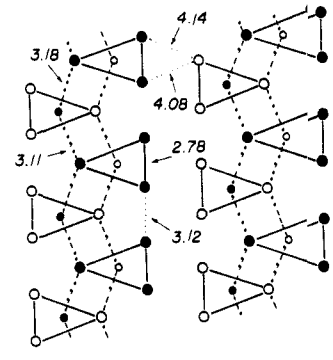

2a

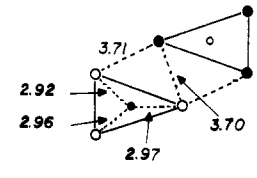

2b

All the above structural features (a – d) of the type B structure become less pronounced in the type A structure. In particular, the structural features (b) and (d) are crucial for the semimetallic properties of $ZrTe_3$, as will be shown in the next section. $ZrTe_3$ is the first example of an MX_3 system with large band dispersion along the interlayer direction.

Electronic Structure

A. Band Structure. Shown in Figure 1 is the band electronic structure of $ZrTe_3$ calculated for its type A structure (i.e., **2a**),

(5) McTaggart, F. K. *Aust. J. Chem.* **1958**, *11*, 445.
(6) Wilson, J. A. *Phil. Trans. R. Soc. London* **1985**, *A314*, 159.
(7) Bayliss, S. C.; Liang, W. Y. *J. Phys. C* **1981**, *14*, L803.
(8) (a) Takahashi, S.; Sambongi, T.; Okada, S. *J. Phys. (Paris) Colloq.* **1983**, *44*, C3-1733. (b) Takahashi, S.; Sambongi, T.; Brill, J. W.; Roark, W. *Solid State Commun.* **1984**, *49*, 1031.
(9) Nakajima, H.; Nomura, K.; Sambongi, T. *Physica* **1986**, *B143*, 240.
(10) (a) Whangbo, M.-H.; Hoffmann, R. *J. Am. Chem. Soc.* **1978**, *100*, 6093. (b) Whangbo, M.-H.; Hoffman, R.; Woodward, R. B. *Proc. R. Soc. London* **1979**, *A366*, 23.
(11) Hoffmann, R. *J. Chem. Phys.* **1963**, *39*, 1397.
(12) (a) Furuseth, S.; Brattas, L.; Kjekshus, A. *Acta Chem. Scand.* **1975**, *A29*, 623. (b) Gjønnes, K. *Ultramicroscopy* **1985**, *17*, 133. (c) Krönnert, W.; Plieth, K. *Z. Anorg. Allg. Chem.* **1965**, *336*, 207.

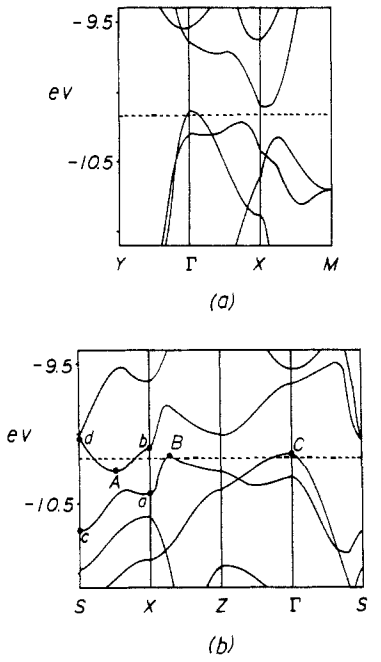

Figure 2. Dispersion relations of some bands in the vicinity of the Fermi level calculated for the type B structure of $ZrTe_3$: (a) $\Gamma \rightarrow X \rightarrow M \rightarrow Y$ cross section, and (b) $\Gamma \rightarrow Z \rightarrow X \rightarrow S$ cross section.

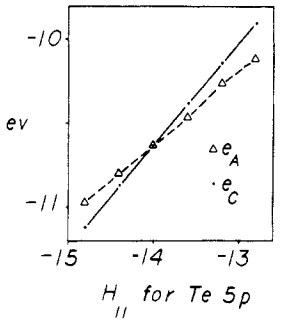

Figure 3. Relative positions of e_A and e_C as a function of the H_{ii} (Te 5p) value.

where the special wave vector points of the first Brillouin zone are defined in **3**. Since a band gap is present between the d-block

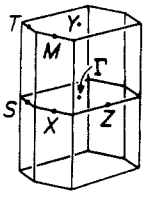

3

bands of Zr and p-block bands of Te, type A $ZrTe_3$ is predicted to be a semiconductor just like other MX_3 chalcogenides. Shown in Figure 2 is the band electronic structure of $ZrTe_3$ calculated for its type B structure, where the p- and d-block bands overlap so that type B $ZrTe_3$ is predicted to be a semimetal as found experimentally.[7,8] To determine how sensitively the occurrence of a semimetallic band structure for type B $ZrTe_3$ depends upon the choice of the atomic parameters, we have repeated our band calculations on type B $ZrTe_3$ with various values of the valence shell ionization potential, H_{ii}, of the Te 5p orbital. Results of these computations are summarized in Figure 3, which plots the energies of points A and C (e_A and e_C, respectively; see Figure 2b for the definition of e_A and e_C) as a function of H_{ii}(Te 5p). The band electronic structure is semimetallic if e_A is lower in energy than e_C. Hence, Figure 3 shows that type B $ZrTe_3$ is predicted to be semimetallic for a wide range of the H_{ii} (Te 5p) values (greater than −14.0 eV). It is clear from Figures 1–3 that the structural characteristics of a type B structure are essential for the semimetallic properties of $ZrTe_3$.

Figure 2 shows that the direct band gap at Γ is about 0.6 eV, which is in reasonable agreement with the lowest transition at 0.435 eV observed from the reflectivity measurements on $ZrTe_3$.[4c] Figure 2 also shows that the bands giving rise to the semimetallic properties overlap by about 0.1 eV, in support of the prediction by Herr and Brill.[4c]

B. Type B Structure and Semimetallic Character. Let us now examine why the type A and type B structures of $ZrTe_3$ are so different in their band electronic structures. The top two occupied p-block bands of type A $ZrTe_3$ (Figure 1) are low-lying in energy, but the corresponding bands of type B $ZrTe_3$ (Figure 2) are high-lying (high enough to cross the Fermi level). At Γ these two bands have primarily the Te 5p orbital character. Shown in **4** and **5** are the nodal properties for the higher and lower lying ones of these two bands at Γ. These band orbitals are antibonding between the Te atoms of adjacent prismatic chains. Therefore, for the type B structure in which there exist short Te···Te contacts (3.48 Å, see **1b**) between the prismatic chains, the extent of the antibonding interactions in **4** and **5** is strong so that the top two p-block bands are significantly raised.

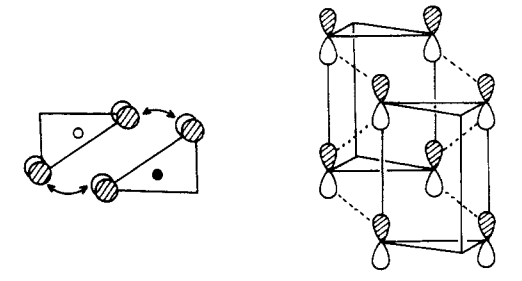

4a 4b

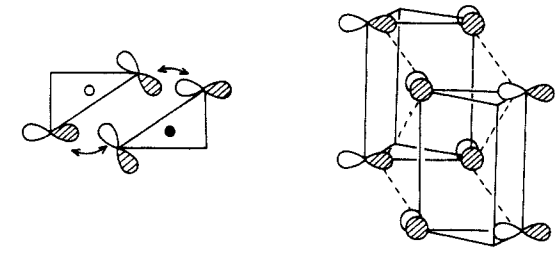

5a 5b

For the top two p-block bands, the band dispersion along X → S (parallel to the interlayer direction Γ → Z) is nearly flat for type A $ZrTe_3$ but dispersive for type B $ZrTe_3$. The partially filled band of type B $ZrTe_3$ along X → S (see Figure 2b) has a minimum (i.e., the point A) in the middle along the X → S line. This is a consequence of the avoided crossing associated with the two levels a and b at X and the two levels c and d at S, as illustrated in **6**. The four energy levels a–d have strong con-

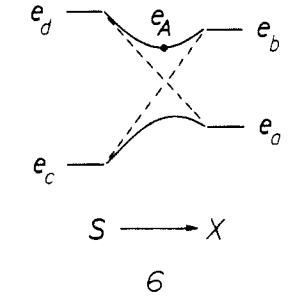

6

tributions from the "in-plane" 5p orbitals (i.e., those perpendicular to the prismatic chain axis) of the Te atoms on the surface of each $ZrTe_3$ layer, so that their band dispersion along the interlayer

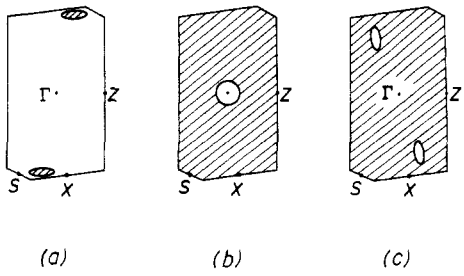

Figure 4. Cross sections of the Fermi surfaces associated with the three partially filled bands of Figure 2: (a) electron pockets associated with the point A, (b) hole pocket associated with the point C, and (c) hole pockets associated with the point B.

direction (i.e., $\Gamma \rightarrow Z$ and $X \rightarrow S$) is strong due both to the short interlayer Te···Te contacts in the type B structure (see **1a**) and to the extended nature of the Te 5p orbitals.

Thus, the top occupied Te 5p-block bands of $ZrTe_3$ lie much higher in energy for the type B than for the type A structure because the shortest interchain and interlayer Te···Te contacts are considerably shorter in the type B structure. Similarly, it is expected for other semiconducting MX_3 chalcogenides that the occupied p-block band of X will lie higher in energy for the type B structure. From this consideration, the band gaps of MX_3 are expected to be greater in type A than in type B structure. In agreement with this prediction, the direct band gaps of type A MS_3 (M = Zr, Hf) are greater than that of type B MS_3 (M = Ti) by about 1 eV (i.e., $\gtrsim$1.9 versus $\sim$0.9 eV).[2b,4] The direct band gap of type A $ZrSe_3$ is 1.1–1.2 eV,[2b,4] which is about 0.8 eV smaller that that of type A ZrS_3. The direct band gap of $HfSe_3$, presumed to be for the type B structure, is 1.02 eV.[2b,4] As mentioned already, $HfSe_3$ exists in both type A and type B forms. The band gap of 1.02 eV for $HfSe_3$ appears to be more appropriate for the type A rather than for the type B structure, since a band gap decrease of $\sim$0.8 eV is expected on going from MS_3 to MSe_3 in the type A structure and since the band gap of MSe_3 is expected to be smaller than that of MS_3 in the type B structure.

C. Fermi Surfaces and the Anisotropic Resistivity Hump. According to Figure 2, type B $ZrTe_3$ has three partially filled bands. All the Fermi surfaces associated with these three bands have the shape of a flat cylinder (i.e., pancake-like). Shown in Figure 4 are the cross sections of these Fermi surfaces on the ΓXZ plane of the first Brillouin zone (see **3**). The two electron pockets of Figure 4a are associated with point A of Figure 2b, and each pocket has the dimension $\sim 0.03a^* \times 0.10b^* \times 0.28c^*$. The hole pocket of Figure 4b (referred to as the hole-1 pocket hereafter) is associated with point C of Figure 2b, and it has the dimension $\sim 0.16a^* \times 0.04b^* \times 0.28c^*$. The two hole pockets of Figure 4c (referred to as the hole-2 pockets hereafter) are associated with point B of Figure 2b, and each pocket has the dimension $\sim 0.12a^* \times 0.10b^* \times 0.10c^*$. The axis of the flat cylinder representing any of the electron and the hole-2 pockets is *perpendicular to* the b^* axis (i.e., the chain direction), but that representing the hole-1 pocket is parallel to the b^* axis. Consequently, the electrical conductivity of $ZrTe_3$ along the chain direction originates primarily from the carriers of the hole-1 pocket, but that *perpendicular to* the chain direction originates mainly from the carriers of the electron and the hole-2 pockets.

The two electron pockets of Figure 4a are nested by the wave vector $q_e \cong 0.95a^* + 0.5c^*$, while the two hole pockets of Figure 4c are nested by the wave vector $q_h \cong 0.7a^* + 0.3c^*$. Thus, a CDW formation associated with q_e and/or q_h would be responsible for the resistivity hump of $ZrTe_3$ at $\sim$63 K. An electron diffraction study of $ZrTe_3$ shows the presence of a CDW with the vector $q_{exp} = 0.93a^* + 0.33c^*$.[13] The a^* component of q_{exp} is close to that of q_e, but the c^* component of q_{exp} is close to that of q_h. From this comparison alone, it is not clear whether the electron pockets and/or the hole-2 pockets cause the resistivity hump at $\sim$63 K.[8] Experimentally, however, holes are found to be associated with the resistivity hump,[8] so that the nesting of the hole-2 pockets are responsible for the occurrence of the CDW at $\sim$63 K. It is important to recall that both the electron and the hole-2 pockets provide carriers leading to the electrical conductivity perpendicular to the chain axis. Consequently, a CDW formation associated either with q_e or q_h would not affect the electrical conductivity along the chain direction. This explains why the resistivity hump in $ZrTe_3$ is observed only along the direction perpendicular to the chain axis.

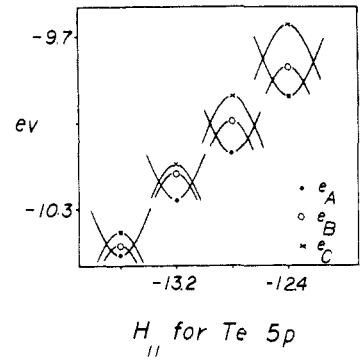

Figure 5. Relative positions of the e_A, e_B, and e_C energy levels as a function of the H_{ii} (Te 5p) value. The parabola around e_A represents the dispersion at the band bottom, while that around e_B or e_C represents the dispersion at the band top.

According to Figure 2b, the occurrence of the two kinds of hole pockets (i.e., the hole-1 and hole-2) stems from the fact that e_B (i.e., the energy at the point B) is closer to e_C than to e_A. This particular feature is necessary to obtain the hole-2 pockets, whose nesting is essential for explaining the resistivity hump of $ZrTe_3$. Figure 5 shows how the relative positions of e_A, e_B, and e_C vary as a function of the H_{ii} (Te 5p) value. The H_{ii} values approximately between −13.4 and −12.6 eV lead to the electron, hole-1, and hole-2 pockets. For other values of H_{ii}, one obtains only the electron and the hole-1 pockets. Since the presence of the hole-2 pockets are essential for the resistivity hump of $ZrTe_3$, only the narrow region of the H_{ii} values (i.e., ca. −13.4 to ca. −12.6 eV) is appropriate for $ZrTe_3$ although other H_{ii} values can produce a semimetallic electronic structure for $ZrTe_3$. Another semimetallic type B MX_3, most likely to be $HfTe_3$[5] if made, might have a resistivity hump from either electron or hole nesting.

Concluding Remarks

Layered transition-metal trichalcogenides MX_3 are classified into type A and type B structures. In the type B structure, short X···X contacts exist between adjacent MX_3 chains in each MX_3 layer and also between adjacent MX_3 layers. These two structural features of the type B structure, plus the diffuse nature (i.e., spatially extended) of Te 5p orbitals, are primarily responsible for the semimetallic properties of $ZrTe_3$. With the H_{ii} (Te 5p) values appropriate for $ZrTe_3$, one obtains three partially filled bands for $ZrTe_3$ that lead to a pair of nested electron pockets, a pair of nested hole pockets, and a hole pocket centered at Γ. The nested electron and the nested hole pockets each have the shape of a flat cylinder whose axis is perpendicular to the b^* axis (the chain direction). Therefore, the carriers of these nested electron and hole pockets are primarily responsible for the electrical conductivity perpendicular to the chain direction. As a consequence, a CDW formation associated with either the nested hole or the nested electron pockets does not affect the electrical conductivity of $ZrTe_3$ along the chain direction. This is the reason why the resistivity hump of $ZrTe_3$ is observed along the direction perpendicular to the chain but not along the chain.

The present study suggests that, for semiconducting MX_3 compounds, the direct band gaps would be smaller for the type B than for the type A structures. In discussing the trends in the optical properties of various semiconducting MX_3 compounds,

(13) Eaglesham, D. J.; Steeds, J. W.; Wilson, J. A. *J. Phys. C* **1984**, *17*, L697.

(14) Ammeter, J. H.; Bürgi, H.-B.; Thibeault, J.; Hoffmann, R. *J. Am. Chem. Soc.* **1978**, *100*, 3686.

therefore, it is important to realize the importance of the difference between the type A and type B structures.

Acknowledgment. E.C. and Y.M. thank the Institut de Chimie Moléculaire d'Orsay (ICMO) for a grant that made possible part of this work and the CIRCE for providing computing facilities. Work at North Carolina State University was in part supported by the U.S. Department of Energy, Office of Basic Energy Sciences, Division of Materials Science under Grant DE-FG05-86-ER45259.

Registry No. $ZrTe_3$, 39294-10-5.

SiC Agostic Interaction with Ti: Origin of Alkenyl Group Distortion in $Ti(C(SiH_2CH_3)=CH_2)X_2^+$. An ab Initio MO Study

Nobuaki Koga and Keiji Morokuma*

Contribution from the Institute for Molecular Science, Myodaiji, Okazaki 444, Japan.
Received June 29, 1987

Abstract: We have optimized the structure of $Ti(C(SiH_2CH_3)=CH_2)(Cl)_2^+$ by an ab initio MO method and found a distorted alkenyl group with a small TiCSi bond angle, a long SiC^γ bond, and a short $Ti\cdots C^\gamma$ distance, all of which are in good agreement with the experiment on $Ti(C(Si(CH_3)_3)=C(C_6H_5)(CH_3))(Cp)_2^+$. Evidence has been found showing that the alkenyl group distortion is a consequence of the donative interaction from the CSi σ bond to a Ti vacant d orbital, similar to the CH···M agostic interaction, and thus it is proposed that this SiC···Ti interaction is called the βSiC agostic interaction. It is suggested that there exist various types of agostic interaction between varieties of σ bonds and the electron-deficient metal with varying structural distortion and stability depending on the donative bonds, metal, ligands, and coordination unsaturation.

Recently the first isolated intermediate $Ti(C(Si(CH_3)_3)=C(C_6H_5)(CH_3))(Cp)_2^+$ (**1**) of a Ziegler catalyst system has been reported by Eisch et al.[1] in the reaction of $C_6H_5C\equiv CSi(CH_3)_3$ with Cp_2TiCl_2 and CH_3AlCl_2. The X-ray structure of **1** shows an interesting distortion in the alkenyl group: a small TiCSi angle of 89° and a short distance between Ti and C^γ of 2.52 Å. They

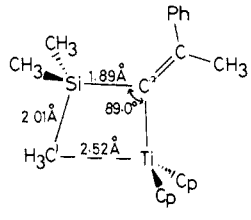

1

have ascribed this distortion to the hyperconjugation between the $C^\alpha Si$ σ bond and a Ti 4p vacant orbital. Although the electron deficiency of the central metal would surely create a driving force for distortion, it is not certain that such a hyperconjugation is operative. The $C^\alpha Si$ bond, which is expected to be longer upon hyperconjugation, is found experimentally not much longer than the standard CSi single bond length: 1.853 Å in vinylsilane[2a] and 1.867 Å in methylsilane.[2b] This is in contrast with the hyperconjugation between a $C^\alpha H$ bond and a metal vacant orbital found in the distorted carbene complexes.[3] The STO-3G calculations have given the long $C^\alpha H$ bond of 1.13–1.18 Å in the model titanium carbene complexes.[3] On the contrary, the SiC^γ bond length in **1** is longer by about 0.1 Å.

It may be noted that the distortion of alkenyl group is similar to that of ethyl groups found experimentally in $Ti(C_2H_5)$-

Table I. Relative Energy (in kcal/mol) of Optimized Structures and Assumed Structures with Undistorted Alkenyl Group

optimized structure		assumed structure		difference
5a	4.0	**10a**	18.1	14.1
5b	0.0[a]	**10b**	17.6	17.6
5c	14.0			

[a] The total energy is −2136.42895 hartrees.

$(dmpe)(Cl)_3$[4a] (**2**) or theoretically in $Ti(C_2H_5)(Cl)_2(PH_3)_2(H)$[5a] (**3**) and $Pd(C_2H_5)(H)(PH_3)$[6] (**4**). The MCC bond angles of the

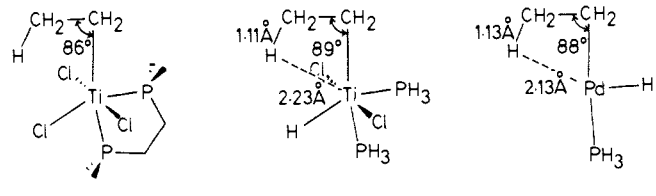

2 **3** **4**

ethyl groups are about 90°, and their $C^\beta H$ bonds are much longer (by 0.3–0.5 Å) than the normal CH bond. These structural features are signs of the intramolecular CH···M interaction, called the agostic interaction.[4c] The origin of the agostic interaction has been found to be the electron donative interaction from a CH σ bond to a metal low-lying vacant orbital.[5,6]

In this paper, we report theoretical evidence on the origin of the alkenyl group distortion in **1**, which is similar to the agostic

(1) Eisch, J. J.; Piotrowski, A. M.; Brownstein, S. J.; Gabe, E. J.; Lee, F. L. *J. Am. Chem. Soc.* **1985**, *107*, 7219.
(2) (a) O'Reilly, J. M.; Pierce, L *J. Chem. Phys.* **1961**, *34*, 1176. (b) Kilb, R. W.; Pierce, L. *Ibid.* **1957**, *27*, 108.
(3) Francl, M. M.; Pietro, W. J.; Hout, R. F., Jr.; Hehre, W. J. *Organometallics* **1983**, *2*, 281.
(4) (a) Dawoodi, Z.; Green, M. L. H.; Mtetwa, V. S. B.; Prout, K. *J. Chem. Soc., Chem. Commun.* **1982**, 802. (b) Dawoodi, Z.; Green, M. L. H.; Mtetwa, V. S. B.; Prout, K. *Ibid.* **1982**, 1410. (c) Brookhart, M.; Green, M. L. H. *J. Organomet. Chem.* **1983**, *250*, 395.
(5) (a) Koga, N.; Obara, S.; Morokuma, K. *J. Am. Chem. Soc.* **1984**, *106*, 4625. (b) Obara, S.; Koga, N.; Morokuma, K. *J. Organomet. Chem.* **1984**, *270*, C33.
(6) Koga, N.; Obara, S.; Kitaura, K.; Morokuma, K. *J. Am. Chem. Soc.* **1985**, *107*, 7109.

0002-7863/88/1510-0108$01.50/0